RSC Advances

PAPER

View Article Online
View Journal | View Issue

Cite this: *RSC Adv.*, 2017, **7**, 15265

Synthesis, characterization and immobilization of N-doped TiO_2 catalysts by a reformed polymeric precursor method†

Han Yu,[ab] Li Ye,*[ab] Tuzi Zhang,[a] Heng Zhou[a] and Tong Zhao*[ab]

A novel synthetic method to prepare N-doped TiO_2 catalysts was studied, by which a stable and homogeneous liquid polymeric precursor was produced, thus the catalysts can be loaded on suitable substrates, making catalysts facilely separated from waste water. The doping ratios and annealing temperatures were optimized by testing photodegradation of the products to methyl orange. To improve the Brunauer–Emmett–Teller surface areas of the catalyst, PEG was grafted to the structure of precursor polymer, by which an increase of 55% in BET surface areas and 20% in the photodegradation efficiencies was achieved. The crystalline phase was measured by X-ray diffraction and structural parameters were calculated by Xpert Highscores. FESEM and HRTEM pictures showed that the average particle size of the nitrogen doped and PEG modified catalyst reached to only 5 nm. X-ray photoelectron spectroscopy showed that nitrogen dope mode was interstitial. Using quartz fabrics as substrate, the loaded catalysts were facilely recycled and reused by 15 times without decay in photodegradation efficiency.

Received 23rd November 2016
Accepted 27th February 2017

DOI: 10.1039/c6ra27187a

rsc.li/rsc-advances

1. Introduction

TiO_2 photocatalysts have attracted considerable attention due to their remarkable performances in environmental applications dealing with water and air purification. Complete and efficient degradation of various organic pollutants including industrial wastewater, domestic sewage or microbial toxins under ultraviolet irradiation can be effectuated by TiO_2 photocatalysts,[1] by decomposing them into CO_2 and H_2O. However, pristine TiO_2 is activated only under UV irradiation due to its wide band gap, limiting the practical efficiency for solar applications. In recent years, the main approaches to modify the photocatalytic ability of TiO_2 catalysts under visible light are based on the methodology of doping chemical reagents including metallic ions like Fe^{3+},[2] Ni^{4+} (ref. 3) or non-metal elements like N,[4–6] F,[7] S.[8,9] Nevertheless, the metal elements doping will compromise thermal stability and shorten lifetime of carriers[10,11] and based on the results of calculation of density of states (DOSs) of doping of non-metal in the anatase TiO_2 crystal, Asahi *et al.*[12] suggested that, the substitutional doping of N could effectively narrow the band-gap by substituting for O 2p states. Since then, significant efforts are being devoted to synthesis of N-doping TiO_2. Several feasible common N-doping pathways have been reported like hydro-thermal synthesis,[13] sol–gel synthesis,[14] micro-emulsion synthesis,[4] powders sintering[15] *etc.* However, these schemes demand long synthetic circle and the as-prepared products are mainly in the form of powders or particles, while the use of aqueous suspension of nanoparticles of TiO_2 for photocatalytic removal of pollutants is not suitable for industrial applications due to the inconvenient and expensive separation of nanoparticles of TiO_2 for reuse.

To avoid the above drawbacks, a novel synthesis scheme, polymeric precursor method[16] was exerted to produce a product existed in the form of stable and homogeneous solution. The precursor showing various advantages because the liquid Ti-precursor can be loaded on suitable reactor substrates, making catalysts facilely separated from treated water.[17] In this paper, visible light active N-doped TiO_2 photocatalyst was prepared *via* polymeric precursor method, and was immobilized on quartz fibers by drop-coating and pyrolysis process. In a typical precursor synthesis method, PEG and a nitrogen-containing compound are introduced as pore templating material for tailor-designing the structural properties of TiO_2 and as nitrogen dopant for its visible light response, respectively. By studying synthetic conditions, precursors structure, pyrolysis conditions and properties of TiO_2 catalysts, the precursor synthesis and pyrolysis process were optimized. To obtain the precise band gap within the TiO_2, first-principles density functional theory (DFT)[18–21] and related calculating software were used to simulate the schematic illustration of density of states of modified samples.

[a]*Laboratory of Advanced Polymer Materials, Institute of Chemistry, Chinese Academy of Sciences, Beijing 100190, P. R. China. E-mail: yeli@iccas.ac.cn; tzhao@iccas.ac.cn*
[b]*University of Chinese Academy of Sciences, Beijing 100049, P. R. China*

† Electronic supplementary information (ESI) available. See DOI: 10.1039/c6ra27187a

2. Experimental

2.1. Synthesis of precursor and powder catalysts

All reagents were used without further purification. N-containing Ti^{4+} resins were prepared by the polymeric precursor method. In a typical procedure, acetamide (Beijing Chemical Co.) was mixed with titanium tetraisopropoxide (Aldrich, TTIP) and drastically stirred at 120 °C for 2 hours. After cooling to 90 °C, acetylacetone (Xilong Chemical Co., Ltd., Hacac) was added and stirred for 10 min. Then, a mixture of H_2O and *n*-propanol (mass ratio of H_2O/*n*-propanol is 1/4) was added dropwise and refluxed for 2 hours. Finally, the solvent was evaporated under reduced pressure, and the obtained viscous precursor was calcined in an air stream at 350, 400, 450 or 500 °C for 15 min (2 hours for undoped TiO_2) at a heating rate of 3 °C min^{-1}. The molar ratio of the TTIP/acetamide/acetylacetone/H_2O was 1.0/0–3.0/0.5/1.0, and the samples were designated with an initial N/Ti ratio (N/Ti = 1.0, 2.0, 3.0 was identified as N-TiO_2-1-*T*, N-TiO_2-2-*T* and N-TiO_2-3-*T* respectively after calcination at temperature *T* °C and N/Ti = 0 was denoted as TiO_2-*T*). PEG containing precursor was obtained in the same way by mixing 12 g PEG-600 (Xilong Chemical Co. Ltd.) with 1 mol TTIP and stirring at 120 °C for 2 hours before its reaction with acetamide (2.0 mol), and the calcined sample was denoted as NP-TiO_2-2-*T*.

2.2. Preparation of catalysts coated fabric

Quartz fabrics (Hubei Feilihua Quartz Glass Co., Ltd) with a size of 50 mm × 30 mm were used as a substrate for fabricating immobilized TiO_2 catalysts and the mass of fabrics were controlled by its tailored thickness. Before coating, the fabrics were heated in muffle at 450 °C to remove the sizing agent. *n*-Propanol solution of the precursor with a Ti mass fraction of 1%, 3% or 5% was spread on the quartz fabrics by drop-coating. The precursor-coated fabrics were dried in vacuum at room temperature and cured at 80 °C with a relative humidity of 80%, followed by calcined at 400 °C for 15 min with a temperature gradient of 3 °C min^{-1}. The prepared TiO_2 catalysts coated quartz fabrics using precursor solutions of different concentration were denoted as QF-1, QF-3 and QF-5 respectively. The coating mass ratio of TiO_2 was determined by weighing the quartz fabrics before and after coating and the loaded catalysts were controlled at the mass of 30 mg.

2.3. Characterization of catalysts

The crystal phases of the catalysts were obtained by X-ray diffraction (Rigaku D/max 2500, Cu Kα source, 40 kV × 200 mA). The nitrogen doping level was confirmed by X-ray photoelectron spectroscopy (XPS, ESCALab220i-XL). The nitrogen content of the catalysts was measured by a TC-306 nitrogen/oxygen analyser (Baoying Technology). Brunauer–Emmett–Teller (BET) surface areas were measured by nitrogen adsorption by induced isotherms at 77 K with a Micromeritics ASAP 2020 instrument. The morphology of the catalysts was analyzed through scanning electron microscopy (SEM, Hitachi SU-8020). For transmission electron microscopy (TEM) analysis, powder samples were suspended in alcohol and sonicated for 10 min before being dispersed onto formvar-coated copper grids. The particle-loaded grids were studied under JEOL JEM-2200 transmission electron microscope operating at an accelerating voltage of 200 kV. The density of states of modified samples was calculated by the VASP software. The ultraviolet-visible diffusion reflectance spectra (UV-vis DRS) were measured by Shimadzu-UV-2600 spectrophotometer. The photoluminescence (PL) spectra were measured with a fluorescence spectrometer (F-4500, HITACHI).

2.4. Measurement of photocatalytic activity

The photocatalytic activity of the catalysts for the oxidation of methyl orange (MO) was tested under visible light illumination. The catalyst powders (30 mg) or the immobilized catalysts (30 mg loaded) were placed in quartz cuvettes and immersed in 30 mL of a methyl orange aqueous solution (15 mg L^{-1}). The cuvettes were placed in a photo-reactor at 25 °C and illuminated by a Xe arc lamp (500 W, cut off wavelength below 420 nm). After the irradiation, the quartz fabric was extracted and washed for 10 times by deionized water. Then it was dried at 100 °C for 30 min before its reutilization. The photocatalytic oxidation of methyl orange was monitored by taking UV-vis measurements (Shimadzu-UV-2600 spectrophotometer) at various light exposure times.

3. Results and discussions

3.1. N-doped TiO_2

3.1.1. Optimization of synthesis parameters. The results of visible light driven photocatalytic degradation of methyl orange are shown in Fig. 1. It is found that the optimal calcination temperature was 450 °C for all precursors despite of the N/Ti ratio, and the optimal N/Ti molar ratio was 2.0. The photocatalytic activity decreased when the N/Ti molar ratio was higher than 2.0, which may be due to the concomitant increase of the recombination rate, consistent with the reported

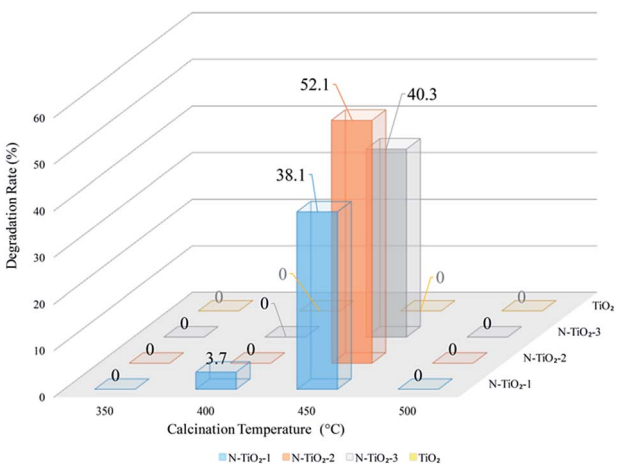

Fig. 1 Degradation of methyl orange under visible light (4 hours) by powder catalysts with different molar ratios of N to Ti and calcination temperatures.

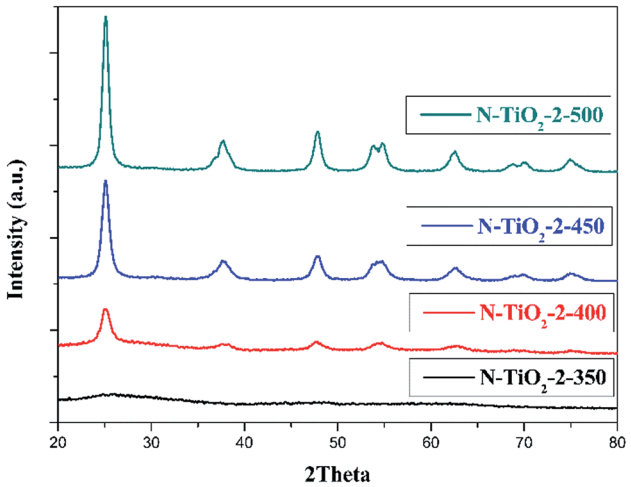

Fig. 2 XRD patterns for N-doped TiO_2 catalysts with different calcination temperatures.

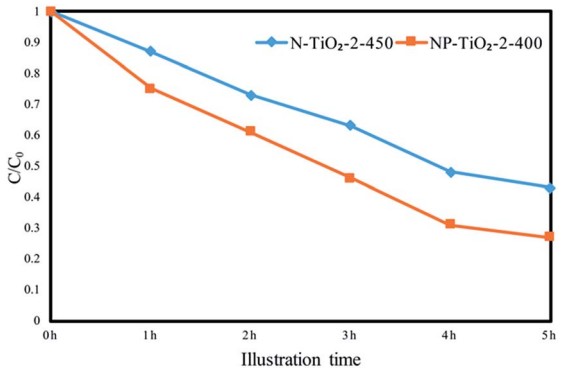

Fig. 3 Time profile of photodegradation of methyl orange under visible light by N-TiO_2-2-450 and NP-TiO_2-2-400.

literature.[22] As a comparison, the undoped samples were also synthesized by the precursor derived method, and all the samples do not show photocatalytic activity under visible light.

3.1.2. XRD characterization. As shown in Fig. 2, the XRD patterns of the as-prepared N-TiO_2-2 precursor which calcined at different temperatures indicate that all samples sintered above 400 °C were predominantly homogeneous anatase phase, and calcination at higher temperature leaded to increase of the crystallinity and crystal size. The XRD pattern of N-doped TiO_2 sintered at 350 °C (N-TiO_2-2-350) shows no crystal phase, while that of the undoped TiO_2 calcined at the same temperature is anatase (Fig. S1†), which suggested that the crystalline process was impeded by doping nitrogen atom.

Rietveld fitting (using Xpert Highscores software-ver. 3.0) and Scherrer equation were applied on the diffraction peaks assigned to the anatase (101) lattice plane to obtain the lattice parameters and crystallite size of the samples. As shown in Table 1, the crystallinity was only 26.56% for catalyst calcined at 400 °C, and increased to 79.07% with a raise of calcination temperature to 450 °C. Further increasing calcination temperature to 500 °C seemed having no obvious contribution to crystallinity, but leaded to the increase of the crystallite size as well as loss of nitrogen. From the XRD results, one can conclude that the scarcity of photocatalytic activity of sample obtained at 400 °C (N-TiO_2-2-400) may be due to its low crystallinity, and that of sample N-TiO_2-2-500 can be attributed to the loss of doped nitrogen under high temperature.[23–25] The sample calcined at 450 °C (N-TiO_2-2-450) appeared to have proper crystallinity as well as nitrogen retention, thus possessing the best photocatalytic activity.

The fitting results listed in Table 1 suggest that the unit cell volume of modified TiO_2 expanded when comparing with that of pure TiO_2, which was due to the atomic radius of nitrogen is larger than that of the oxygen. The results were consistent with the previous literature[25] and hint that nitrogen atoms were successfully incorporated into TiO_2 lattice.

3.2. PEG modified catalysts

Studies showed that surface areas of the catalysts have a direct impact on the photocatalytic activity of the catalyst, so PEG-600, a pore-former used was grafted to the Ti atom during synthesis process (pre-modified) or directly mixed with the prepared precursor solution (post-modified) to increase the BET surface area of the precursor derived TiO_2 catalyst. To facilitate the comparison, the quantity of PEG-600 added to the two samples was equal.

Table 1 XRD, ICP-AES and BET data for N-doped TiO_2

Sample	Crystal phase	Crystallite size (Å)	Lattice parameter (Å)	Refinement agreement indices	Crystallinity (%)	Nitrogen content (wt%)
N-TiO_2-2-350	n/a	n/a	n/a	n/a	0	0.082
N-TiO_2-2-400	Anatase (ICDD: 01-086-1156)	97	$a = b = 3.794704$, $c = 9.661116$	$R_{exp} = 12.43629$, $R_p = 12.99809$, $R_{wr} = 17.14108$	26.56	0.423
N-TiO_2-2-450	Anatase (ICDD: 01-073-1764)	110	$a = b = 3.802327$, $c = 9.674527$	$R_{exp} = 13.87848$, $R_p = 18.25484$, $R_{wr} = 26.22595$	79.07	0.220
N-TiO_2-2-500	Anatase (ICDD: 01-086-1157)	123	$a = b = 3.809623$, $c = 9.637403$	$R_{exp} = 12.26462$, $R_p = 16.62596$, $R_{wr} = 23.94779$	79.47	0.039
TiO_2-450	Anatase (ICDD: 01-086-1157)	150	$a = b = 3.781225$, $c = 9.485132$	$R_{exp} = 14.876$, $R_p = 15.282$, $R_{wr} = 20.730$	100	0
NP-TiO_2-2-400	Anatase (ICDD: 01-078-2486)	95	$a = b = 3.80572$, $c = 9.667077$	$R_{exp} = 14.7501$, $R_p = 15.23591$, $R_{wr} = 21.35636$	67.73	0.213

Table 2 BET data and photo degradation rates of N-doped TiO_2 catalysts

Sample	S_{BET} (m^2 g^{-1})	Degradation rate[a] (%)
N-TiO_2-2-450	109.24	52
NP-TiO_2-2-400	170.31	69
N-TiO_2-2-PEG-400	169.35	59

[a] Degradation of methyl orange under visible light (4 hours).

3.2.1. Photocatalytic property and BET characterization. The visible light driven photocatalytic degradation results (Fig. S2†) shows that 400 °C is the optimal temperature for PEG-grafting precursors. When compared with unmodified sample, as shown in Fig. 3, the degradation capacity of PEG pre-modified TiO_2 catalysts calcined at 400 °C was higher than that of the unmodified sample throughout the photo-degradation process, and the degradation rate was 73% for 5 h irradiation, while that of unmodified sample was only 57%.

As shown in Table 2, the BET surface areas of the two samples (NP-TiO_2-2-400 and N-TiO_2-2-PEG-400) with different PEG addition methods were almost identical, both improved by 55% comparing with that of the sample without PEG (N-TiO_2-2-450). And both samples showed an improved photocatalytic activity comparing with that of sample without PEG. Moreover, the pre-modified sample NP-TiO_2-2-400 showed a higher photocatalytic activity than that of the post-modified sample N-TiO_2-2-PEG-400. This phenomenon may be interpreted by pyrolysis of PEG. When PEG was added during the synthesis process, PEG-600 was supposed to be grafted to the precursor, thus during the following thermal process, the pores formed by decomposition of the grafted PEG would be distributed homogenously in the catalyst. However, PEG aggregation was supposed to occur during the calcination due to its poor dissolvability in precursor solution and deficient mixing uniformity in the post-modified sample, resulting in the interior homogeneity of its pore distribution.

3.2.2. Characterization of crystalline structure and morphology. XRD results (Fig. 4) showed that all the PEG-grafted samples calcined at 350–500 °C were predominantly homogeneous anatase phase. Comparing with the XRD patterns of samples without PEG, one can conclude that the addition of PEG-600 can lower the crystallization temperature without changing the crystallization phase of the resulting catalysts. As shown in Table 1, the crystallinity of sample NP-TiO_2-2-400 was 67.73%, which was far higher than that of sample without PEG but calcined at the same temperature (N-TiO_2-2-400). The post-modified sample also behave a lower crystallization temperature comparing with that of the unmodified sample (Fig. S3†), which may be due to the induced crystallization effect of PEG. The results was similar as the study of French *et al.*,[27] who reported that PEG could behave as the crystal nucleus for heterogeneous nucleation.

To study the influences of grafted PEG to the morphology of N-doped TiO_2, FESEM and HRTEM images of samples N-TiO_2-2-450 and NP-TiO_2-2-400 which have the best photocatalytic activity were measured and shown in Fig. 5. From the results one can note that both the samples show spherical nano-particles (Fig. 5a and b) stacking into grape-like aggregates. The particle size of sample N-TiO_2-2-450 ranged from 10–20 nm, and that of sample NP-TiO_2-2-400 was about 5 nm. The HRTEM images illustrate that the nano-particles were comprised of highly crystallized anatase with lattice of 0.35 nm which was corresponding to the (101) crystallographic plane of TiO_2. Particle size measured in HRTEM image (Fig. 5d) for sample NP-TiO_2-2-400 was smaller than that of N-TiO_2-2-450 (Fig. 5c) and it was consistent with the data obtained from FESEM images.

3.2.3. Chemical structure. The chemical composition and elemental valence of NP-TiO_2-2-400 was detected by XPS analysis. The XPS survey spectra (Fig. 6a) shows three characteristic peaks ascribed to Ti, O and N respectively. High resolution XPS spectra for Ti 2p (Fig. 6b) shows two peaks corresponding to

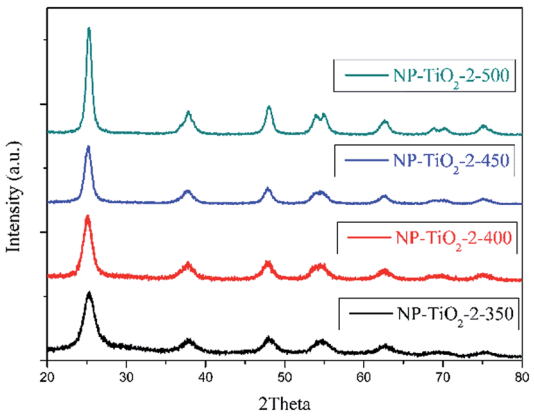

Fig. 4 XRD patterns for PEG pre-modified samples annealed at different temperatures.

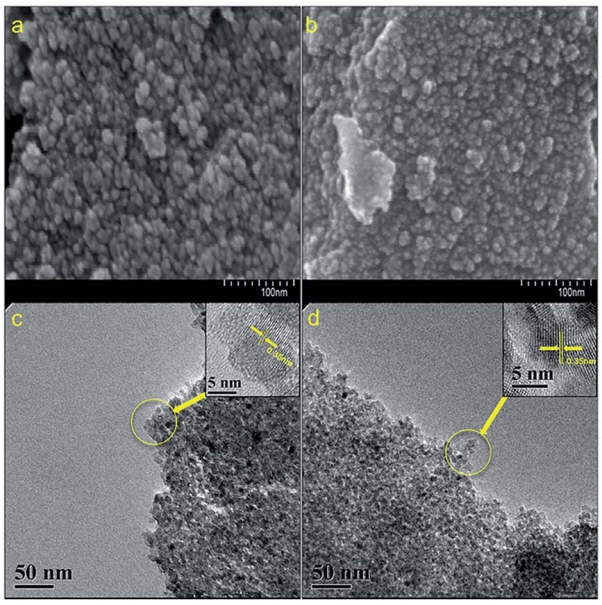

Fig. 5 FESEM images for (a) N-TiO_2-2-450 and (b) NP-TiO_2-2-400; HRTEM images for (c) N-TiO_2-2-450 and (d) NP-TiO_2-2-400.

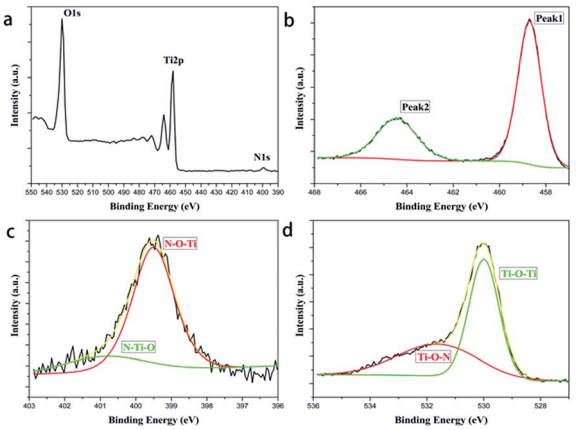

Fig. 6 Fitted XPS spectra of (a) survey, (b) Ti 2p, (c) N 1s and (d) O 1s for NP-TiO_2-2-400.

binding energies of Ti $2p_{1/2}$ and Ti $2p_{3/2}$ at 464.3 eV and 458.6 eV, respectively. The binding energy difference of the two peaks ($\Delta = 5.7$ eV) indicates that Ti existed in forms of Ti^{4+}.[26] As shown in Fig. 6c, the N 1s peak of NP-TiO_2-2-400 could be deconvoluted into two peaks located in 399.6 eV and 400.7 eV, which was attributed to N–O–Ti and N–Ti–O, respectively.[28,29] The results indicate that N atoms were incorporated into interstitial sites, and no substitutional N atoms exited in the form of Ti–N–Ti.[12,30–32] In correspondence with that of N 1s, the O 1s XPS spectra also shows the peak of Ti–O–N located in 531.7 eV, which confirmed the interstitial doped form.[4,33]

3.2.4. Optical property. To investigate the optical property including the capacity of photon reaping, electron–hole pairs trapping, migration and transfer, and to obtain the life track which implement high impact on photocatalysis, photoluminescence emission spectra[34] and UV-vis absorption spectrum were investigated.

UV-vis absorption spectrum shows photon reaping capacity of N-doped TiO_2 catalysts mainly by comparing optical absorption edges. Fig. 7 shows the UV-vis diffuse reflectance spectra of undoped and nitrogen doped TiO_2 photocatalysts. As shown in Fig. 7b, absorption edge of sample N-TiO_2-2-450 exhibits an evident red shift. However, the absorption edges of sample NP-TiO_2-2-400 and N-TiO_2-2-PEG-400 show blue shift compared with sample N-TiO_2-2-450. Further study is required to fathom the effect.

Moreover, nitrogen doped samples still possessed obvious absorption intensity after 400 nm while the pristine TiO_2 showed hardly any absorption in this spectrum. Thus, the addition of nitrogen can not only enhance lifetime of charge carriers but also visible light usage effectiveness.

The PL spectra (Fig. 8) shows that the PL intensities of all N-doped catalysts were way lower than the undoped one, indicating that doping nitrogen enhanced the efficiency of charge separation and transfer from valence band to conduction band and the number of recombination center also declined since the spectrum reflects the photon emission signals from the recombination of secondarily excited electron–hole pairs.

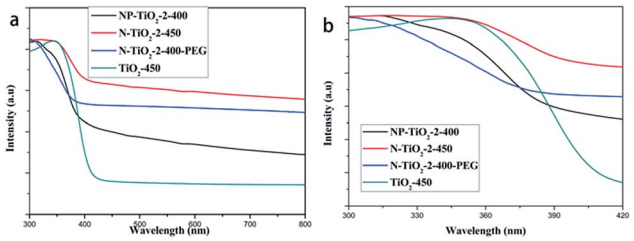

Fig. 7 UV-vis absorption spectrum for N-doped and pristine TiO_2 catalysts.

Moreover, PL intensity of sample NP-TiO_2-2-400 was further lower than that of the other two N-doped samples, which indicated that improved capacity of electron–hole pairs migration was achieved by grafting PEG to Ti atom. The relatively high capacity of electron–hole pairs migration made the photoactivity of the pre-modified sample be higher than that of the post-modified sample with the same BET surface area.

3.2.5. Energy band calculation. To investigate the change of band gap structure and pinpoint the effect of introduced interstitial nitrogen to it, first-principles density functional theory (DFT) was utilized to calculate relevant data.[21] The schematic illustration of model structure for as-prepared undoped TiO_2 and sample NP-TiO_2-2-400 (Fig. 9a and b) was constructed according to the method of Di Valentin *et al.*[35] The interstitial nitrogen was bound to one lattice oxygen, interacting with lattice titanium in the form of Ti–NO or Ti–ON which was consistent with XPS results. The calculated DOS indicates that a small mid-gap localized state due to the substantially low doping ratio was generated by interstitial N through N–O–π bond and it was about 1.5 eV to the valence band maximum. DFT method is prone to narrow the band gap of semiconductor, thus following the reported literature,[21] the "scissor operator" treatment was applied to correct the calculated results which shifted the conduction band by 1.5 eV, thus it can be concluded that the doped nitrogen narrows the factual band gap to 1.7 eV. Although the mid-gap state was seemingly relatively negligible,

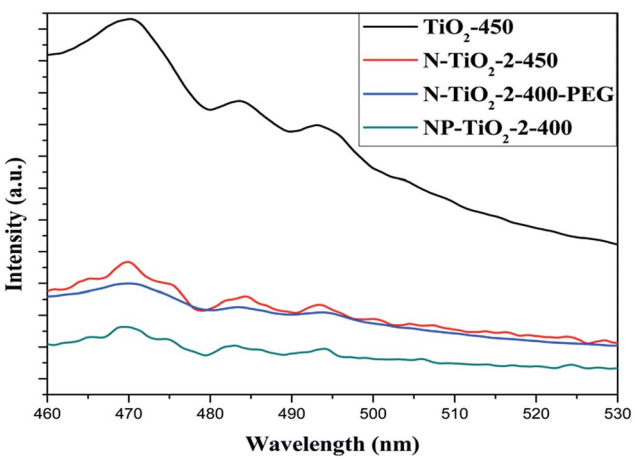

Fig. 8 Photoluminescence emission spectra for TiO_2 catalysts excited at 280 nm at 20 °C.

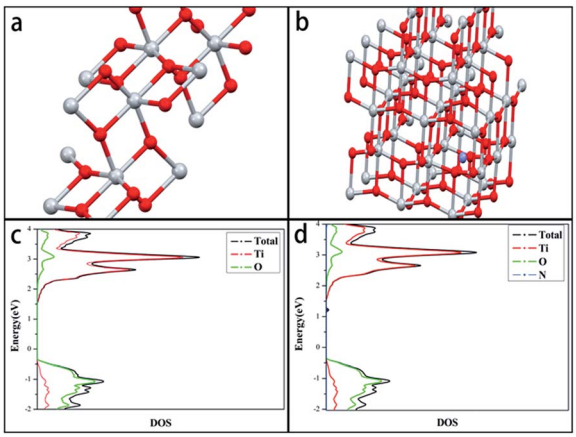

Fig. 9 Schematic illustration of crystal lattice structure of (a) undoped TiO_2, (b) NP-TiO_2-2-400 (red: oxygen atoms; gray: titanium atoms; purple: nitrogen atoms) and their respective calculated DOS ((c) undoped TiO_2, (d) NP-TiO_2-2-400).

it bestowed significant enhancement of photocatalysis on the doped TiO_2 under visible light.

3.3. Cycling tests of the TiO_2 coated quartz fabric

The catalysts coated quartz fabrics using precursors of different Ti mass fraction were prepared. Detailed preparation parameters for QF-1, QF-3 and QF-5 were listed in Table S1.† To ensure the supported catalysts have equal mass as well as the good uniformity (the mass ratio of precursor solution to quartz fabric should be greater than 4), the mass of quartz fabric for QF-5 was halved. The coating mass ratio of QF-1 and QF-3 was 20% while that of QF-5 was 40%.

Cycling tests of the photodegradation under visible light were imposed on the TiO_2 catalysts coated fabric (Fig. 10). As shown in Fig. 10, QF-1 exhibited reusable stability but low photocatalytic activity, while QF-5 showed high photocatalytic activity at the first round, but plummeted after recycling. The sharp decreasing photocatalytic activity of QF-5 was due to the high load ratio,

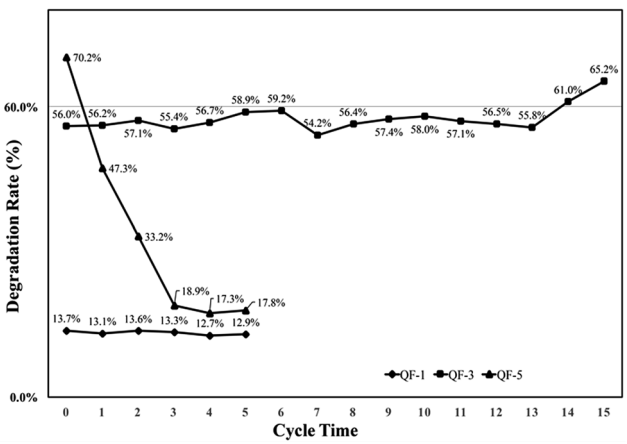

Fig. 10 Cycling tests of photodegradation of methyl orange of catalysts coated quartz fabric.

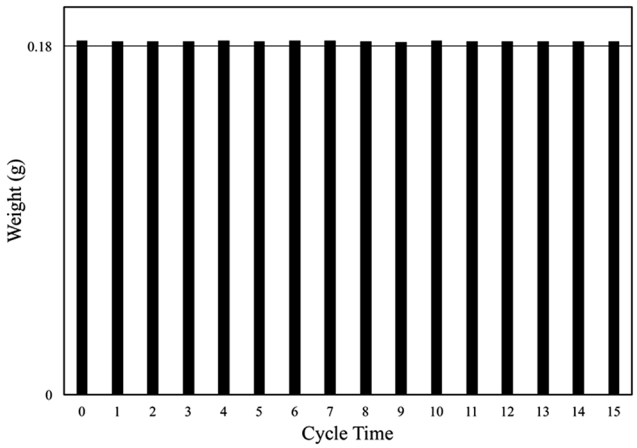

Fig. 11 Mass of QF-3 after each cycle of photodegradation test.

which made the supported catalysts unstable and facilitated their shedding. QF-3 showed high photocatalytic activity as well as favorable cycle stability. Both the photocatalytic activity and the mass of QF-3 were not decreased after reused for 15 times (Fig. 11), indicating that the immobilized catalysts were firmly clung to quartz fiber and retained their photocatalytic capacity.

4. Conclusion

Through the novel polymeric precursor method provided by this research, immobilized visible light active TiO_2 photocatalysts were successfully prepared, and the new idea derived from this method could be used for resolving the two bottleneck problems that restrict the practical applications of TiO_2, low photocatalysis under visible light and difficulties in the recycle and reuse of catalysts. The XPS and DFT calculation results revealed that the nitrogen narrowed the origin band gap of anatase TiO_2 to 2.8 eV by generating mid-gap states in the interstitial doped form.

Additionally, this synthesis process also showed compatibility with various modification methods like multi-elements doping or pore forming. For instance, in this work PEG-600 was added in as a porogen. Compared with the unmodified sample, PEG improved BET surface areas of catalysts by 55% and photodegradation rates of methyl orange by 33% when irradiated under visible light for 4 hours. Moreover, grafting PEG onto the titanium increased the capacity of electron–hole pairs separation and migration, boosting the number of charge carriers and extending their lifespans simultaneously. Thus, we can attempt to add more dopants or templates to prepare porous TiO_2 photocatalysts with higher surface areas and better performances in visible-light photodegradation.

Acknowledgements

This work was financially supported by National Science Foundation of China (No. 21604090 and No. 51403218). The authors are sincerely grateful for the quantum calculation work done by Professor Yuanping Yi, Institute of Chemistry, Chinese Academy of Sciences.

References

1 M. R. Hoffmann, S. T. Martin, W. Y. Choi and D. W. Bahnemann, *Chem. Rev.*, 1995, **95**, 69–96.
2 W. Zhao, W. H. Ma, C. C. Chen, J. C. Zhao and Z. G. Shuai, *J. Am. Chem. Soc.*, 2004, **126**, 4782–4783.
3 T. Ohno, S. Y. Lee and Y. Yang, *Rare Met.*, 2015, **34**, 291–300.
4 Y. Cong, J. Zhang, F. Chen and M. Anpo, *J. Phys. Chem. C*, 2007, **111**, 6976–6982.
5 J. Yuan, M. Chen, J. Shi and W. Shangguan, *Int. J. Hydrogen Energy*, 2006, **31**, 1326–1331.
6 J. Ananpattarachai, P. Kajitvichyanukul and S. Seraphin, *J. Hazard. Mater.*, 2009, **168**, 253–261.
7 H. Barndok, M. Pelaez, C. Han, W. E. Platten III, P. Campo, D. Hermosilla, A. Blanco and D. D. Dionysiou, *Environ. Sci. Pollut. Res.*, 2013, **20**, 3582–3591.
8 T. Ohno, M. Akiyoshi, T. Umebayashi, K. Asai, T. Mitsui and M. Matsumura, *Appl. Catal., A*, 2004, **265**, 115–121.
9 T. Umebayashi, T. Yamaki, H. Itoh and K. Asai, *Appl. Phys. Lett.*, 2002, **81**, 454–456.
10 H. Yamashita, M. Honda, M. Harada, Y. Ichihashi, M. Anpo, T. Hirao, N. Itoh and N. Iwamoto, *J. Phys. Chem. B*, 1998, **102**, 10707–10711.
11 Y. Wang, H. Cheng, Y. Hao, J. Ma, W. Li and S. Cai, *Thin Solid Films*, 1999, **349**, 120–125.
12 R. Asahi, T. Morikawa, T. Ohwaki, K. Aoki and Y. Taga, *Science*, 2001, **293**, 269–271.
13 Y. Cheng, M. Zhang, G. Yao, L. Yang, J. Tao, Z. Gong, G. He and Z. Sun, *J. Alloys Compd.*, 2016, **662**, 179–184.
14 S. Livraghi, M. C. Paganini, E. Giamello, A. Selloni, C. Di Valentin and G. Pacchioni, *J. Am. Chem. Soc.*, 2006, **128**, 15666–15671.
15 K. Kobayakawa, Y. Murakami and Y. Sato, *J. Photochem. Photobiol., A*, 2005, **170**, 177–179.
16 G. B. Soares, B. Bravin, C. M. P. Vaz and C. Ribeiro, *Appl. Catal., B*, 2011, **106**, 287–294.
17 D. A. H. Hanaor and C. C. Sorrell, *Adv. Eng. Mater.*, 2014, **16**, 248–254.
18 G. Kresse and J. Hafner, *J. Non-Cryst. Solids*, 1993, **192**, 222–229.
19 G. Kresse and J. Hafner, *Phys. Rev. B: Condens. Matter Mater. Phys.*, 1993, **48**, 13115–13118.
20 G. Kresse and J. Furthmüller, *Comput. Mater. Sci.*, 1996, **6**, 15–50.
21 X. Chen, L. Liu, P. Y. Yu and S. S. Mao, *Science*, 2011, **331**, 746–750.
22 J. Zhang, Y. Wu, M. Xing, S. A. K. Leghari and S. Sajjad, *Energy Environ. Sci.*, 2010, **3**, 715–726.
23 C. Y. Teh, T. Y. Wu and J. C. Juan, *Catal. Today*, 2015, **256**, 365–374.
24 G. Zhang, Y. C. Zhang, M. Nadagouda, C. Han, K. O'Shea, S. M. El-Sheikh, A. A. Ismail and D. D. Dionysiou, *Appl. Catal., B*, 2014, **144**, 614–621.
25 T. Matsumoto, N. Iyi, Y. Kaneko, K. Kitamura, S. Ishihara, Y. Takasu and Y. Murakami, *Catal. Today*, 2007, **120**, 226–232.
26 L. Zeng, Z. Lu, M. Li, J. Yang, W. Song, D. Zeng and C. Xie, *Appl. Catal., B*, 2016, **183**, 308–316.
27 A. C. French, A. L. Thompson and B. G. Davis, *Angew. Chem., Int. Ed.*, 2009, **48**, 1248–1252.
28 H. X. Li, J. X. Li and Y. I. Huo, *J. Phys. Chem. B*, 2006, **110**, 1559–1565.
29 A. Fujishima, X. Zhang and D. A. Tryk, *Surf. Sci. Rep.*, 2008, **63**, 515–582.
30 H. Irie, Y. Watanabe and K. Hashimoto, *J. Phys. Chem. B*, 2003, **107**, 5483–5486.
31 X. B. Chen, Y. B. Lou, A. C. S. Samia, C. Burda and J. L. Gole, *Adv. Funct. Mater.*, 2005, **15**, 41–49.
32 S. Sakthivel and H. Kisch, *ChemPhysChem*, 2003, **4**, 487–490.
33 M. Pelaez, P. Falaras, V. Likodimos, A. G. Kontos, A. A. de la Cruz, K. O'Shea and D. D. Dionysiou, *Appl. Catal., B*, 2010, **99**, 378–387.
34 J. L. Zhang, Y. Hu, M. Matsuoka, H. Yamashita, M. Minagawa, H. Hidaka and M. Anpo, *J. Phys. Chem. B*, 2001, **105**, 8395–8398.
35 C. Di Valentin, E. Finazzi, G. Pacchioni, A. Selloni, S. Livraghi, M. C. Paganini and E. Giamello, *Chem. Phys.*, 2007, **339**, 44–56.